Appl. Phys. A
DOI 10.1007/s00339-014-8268-8

Applied Physics A
Materials Science & Processing

Background gas collisional effects on expanding fs and ns laser ablation plumes

S. S. Harilal · N. Farid · J. R. Freeman · P. K. Diwakar · N. L. LaHaye · A. Hassanein

Received: 4 November 2013 / Accepted: 16 January 2014

Abstract The collisional effects of a background gas on expanding ultrafast and short pulse laser ablation plumes were investigated by varying background pressure from vacuum to atmospheric pressure levels. For producing Cu ablation plumes, either 40 fs, 800 nm pulses from a Ti: Sapphire laser or 6 ns, 1,064 nm pulses from a Nd:YAG laser were used. The role of background pressure on plume hydrodynamics, spectral emission features, absolute line intensities, signal to background ratios and ablation craters was studied. Though the signal intensities were found to be maximum near to atmospheric pressure levels, the optimum signal to background ratios are observed ~20–50 Torr for both ns and fs laser ablation plumes. The differences in laser–target and laser–plasma couplings between ns and fs lasers were found to be more engraved in the crater morphologies and plasma hydrodynamic expansion features.

1 Introduction

Laser ablation (LA) is a technique of great interest in a wide variety of fields. In analytical chemistry, LA is frequently used as a sample introduction technique for mass spectrometry (e.g., LA-ICP-MS), as well as being used to perform laser-induced breakdown spectroscopy (LIBS) [1–3]. LA has also been used in fields such as pulsed laser deposition (PLD), nanoparticle production, and micromachining. However, excitation of laser pulse duration is a very important consideration in these applications. The mechanism of ablation varies greatly from ns to fs-LA. In ns-LA, the front edge of the laser pulse heats the target, causing melting and removal of material, forming the plasma, while the rest of the plume simply serves to reheat the plasma. Meanwhile, fs-LA mechanisms have not been determined as thoroughly, but the two main ionization mechanisms are collisional impact ionization and photoionization [4, 5]. Material removal occurs through either Coulomb explosion, phase explosion or thermal vaporization [6]. An important factor in fs-LA is that the pulse duration is considerably shorter than both the electron–ion relaxation and the heat conduction times. These differences make some laser pulse durations more advantageous than others for certain applications. In LA-ICP-MS, fs-LA produces better results than ns-LA due to the formation of smaller particles and the reduction of heating effects [2]. In LIBS, fs-LA produces lower continuum emission and an atomic plume in comparison to ns-LA [7].

Most LA applications are performed in the presence of an ambient gas. The function of the background gas varies with respect to the application, for example: as a moderator of particles or generating reactive species in PLD, emission excitation agent in LIBS, nucleation and flushing purposes in LA-ICP-MS, agent for nucleation in nanoparticle synthesis, etc. The LA plumes expand freely and adiabatically in vacuum. The entire hydrodynamics of plume expansion becomes much more complex in the presence of an ambient gas causing effects such as plume splitting, sharpening, confinement, and the formation of internal plume structures [8]. In the presence of moderate to high

S. S. Harilal (✉) · N. Farid · J. R. Freeman · P. K. Diwakar · N. L. LaHaye · A. Hassanein
Center for Materials Under Extreme Environment, School of Nuclear Engineering, Purdue University, West Lafayette, IN 47907, USA
e-mail: hari@purdue.edu

N. Farid
School of Physics and Optical Engineering, Dalian University of Technology, 116024 Dalian, China

Published online: 30 January 2014

ambient pressures, a shock wave will be formed at the interface between the plume and ambient medium at the start of ablation and continue to expand until the back pressure from the ambient gas matches the pressure of the plasma plume [9]. Computational modeling of ns-LA expansion in an ambient gas has been achieved and found to match closely with experimental results [9]. However, the complexity of fs plasma formation makes it difficult to model in the presence of an ambient gas, and further studies are necessary to fully understand the plasma hydrodynamics.

Even though extensive research has been carried out on the role of ambient pressure on dynamics of ns-LA [10, 11], its effect on fs-LA plume hydrodynamics has been studied scarcely. In this article, we investigated the collisional effects generated by changes in background gas pressures for LA plumes with a special emphasis on the differences in ns- and fs-generated plumes. We used a multitude of diagnostic tools for identifying the various differences in ns- and fs-LA plumes under varying air background pressures.

2 Experimental

The results presented in this article have been obtained from ns and fs laser ablation plumes at varying pressure environments in a vacuum chamber. Chamber pressure was regulated using a combination of turbomolecular and roughing-line pumps. Plasma generation of ns laser-produced plasma (LPP) was accomplished using an Nd:YAG laser with a laser pulse duration of 6 ns at its fundamental wavelength of 1064 nm. Ultrafast LA plumes were generated using a mode-locked Ti–Sapphire oscillator, amplified using a chirped pulse amplifier. This combination produces 40-fs pulses, measured using an autocorrelator, at a wavelength centered at 800 nm. Due to a pulse duration difference of approximately five orders of magnitude between typical ns and fs laser systems, comparative laser ablation studies using similar laser power densities are not possible. For analytical applications, power density for fs lasers is typically in the $\sim 10^{13}$ to 10^{14} W/cm^2 range, while for ns lasers this is often in the $\sim 10^9$ to 10^{10} W/cm^2 range. For the present studies, we used laser intensities of 5×10^9 W/cm^2 (100 mJ/pulse) and 3×10^{14} W/cm^2 (4.5 mJ/pulse) for ns- and fs-LA, respectively.

The diagnostic tools used in this study include optical emission spectroscopy (OES), fast-gated imaging and crater morphology analysis. Visible light spectral emission data have been captured using a triple grating 0.75-m focal length spectrograph, and an intensified charge-coupled device (ICCD) is used for recording the wavelength dispersed signal. Imaging of laser ablation plumes is accomplished using an ICCD. Emission spectra and images can be collected from the ICCD in either a time-resolved (offering a minimum gate width of 2 ns) or time-integrated manner by varying gate width with specified gate delays after initial plasma formation. Gate width and gate delay parameters are specified for each experimental data set provided in this article. Ablation crater images are obtained using a scanning electron microscope (SEM) after several laser shots on the target.

3 Results and discussion

We used gated imaging techniques with the ICCD for comparing expansion dynamics of ns and fs laser ablation plumes under varying background pressures. Figure 1 gives the differences in plume expansion generated by ns and fs lasers at various instants during its expansion and at various pressure levels. All the images are spectrally integrated in the visible region and normalized to its own maximum intensity. Previous studies highlighted the differences in expansion dynamics of ns and fs LPP in vacuum [7]. It has been showed that fs-LA provided two distinct components expansion features viz. plasma and nanoparticle plumes, separated by the time of appearance [12] [13]. The persistence of plasma and nanoparticle plumes is $\sim$500 ns and $\sim$100 μs, respectively, propagating with velocities differing by 25 times [12]. In the present study, we concentrated the plume dynamics rather than nanoparticle emission dynamics and hence the time of studies is restricted up to a few μs. Instead of spherical expansion noticed in ns LPP, fs LPP plumes are found to expand with a much stronger forward bias in directions normal to the target surface. Forward-directed expansion of fs laser plumes can be understood by considering pressure confinement due to strong overheating in the laser impact zone and narrower angular distribution of ions and evaporated mass in comparison with ns LPPs [14]. Though both the plumes expand freely and rapidly in the forward direction, the persistence is found to be significantly higher for ns-LA plumes compared to fs-LA plumes. This could be related to increased laser–plasma coupling, rather than laser–target coupling, as seen in ns-LA with high irradiances similar to this study the most of the laser energy is used for heating the plasma rather than coupling with the target [15, 16]. However, it has to be mentioned here that a direct comparison between the self-emission intensities is rather misleading considering the vast differences in the laser energy and power densities used in the present studies for ns- and fs-LA. Nevertheless, the present studies provide a comprehensive picture of hydrodynamic expansion features of ns- and fs-LA

under typically used laser intensity levels for most of their applications.

The interaction between the plasma species and ambient gas species is found to be similar to vacuum case until the background gas pressure reaches 10 s of mTorr pressure levels. The images given at 100 mTorr clearly show the collisional effect indicated by enhanced emission at extended regions of the plume. Enhanced emission can be explained by increased collisions between plume species with ambient gas species resulting in the excitation of plume species. In this pressure range both ns- and fs-LA plumes showed spherical geometry. However, the differences in the plume hydrodynamics are more distinct with increasing pressure. For example, at 500 mTorr, the fs-LA plumes are still maintaining the spherical shape while the ns-LA plumes show sharpening effects. At 1–10 Torr pressure levels, instabilities in the plume front are evident for ns-LA while the reduction in aspect ratio is more

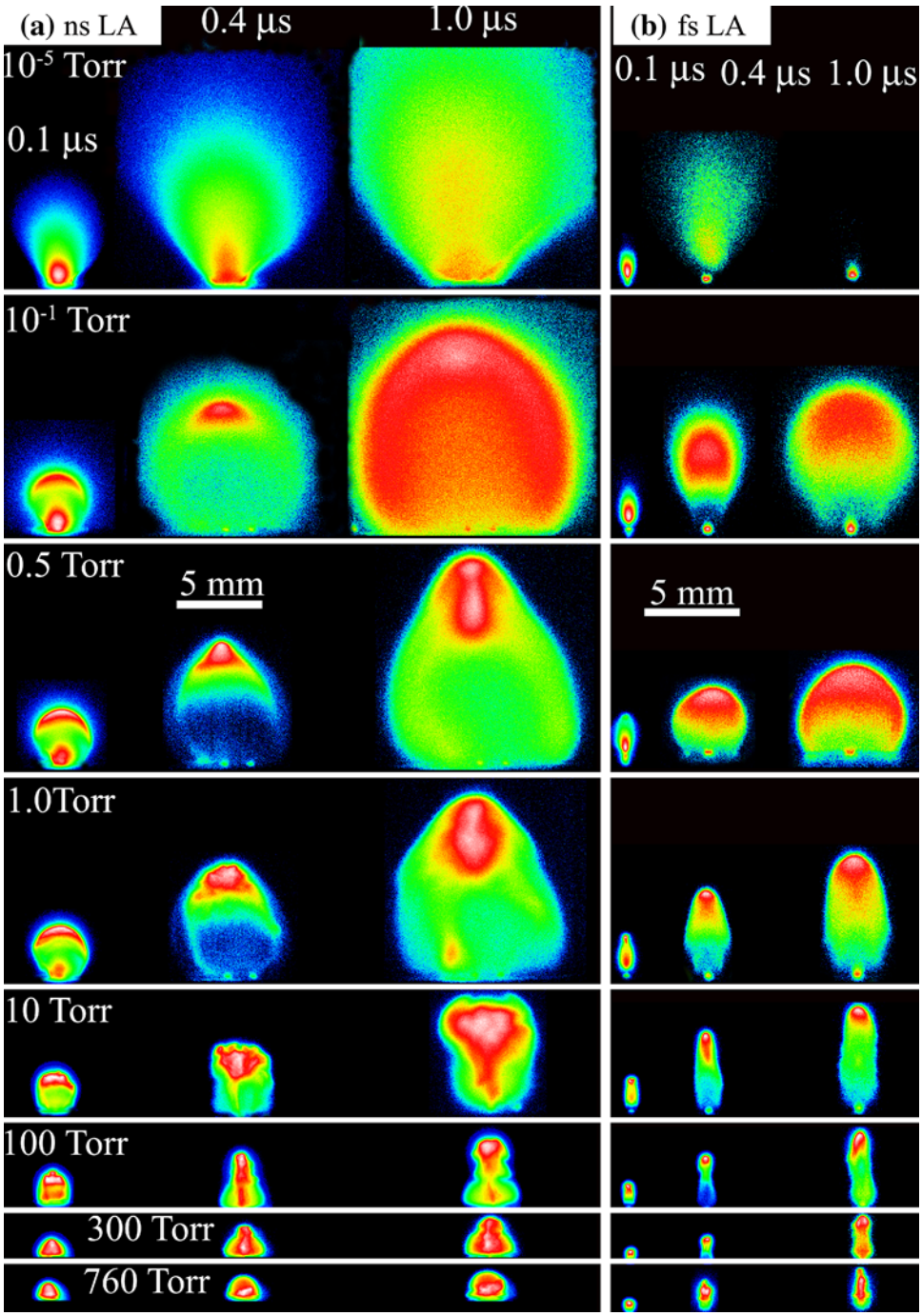

Fig. 1 Time-resolved and spectrally integrated images of ns (*left*) and fs (*right*) laser ablation plumes at various air background pressure levels. The laser intensities used for generating plumes are 5×10^9 and 3.5×10^{14} W/cm^2 for ns- and fs-LA plumes, respectively

evident for fs-LA plumes. The instabilities at the interface of two fluids (i.e., plasma and ambient gas) for ns-LA plumes are probably caused by the Rayleigh–Taylor instability [8]. At still higher pressures, both the plasmas are confined and effective length is reduced to a few mm. However, even at higher-pressure levels, the fs plumes showed more cylindrical geometry compared to ns-LA plumes. Compared to ns-LA, in fs-LA most of the ions, as well as ablated mass, are ejected from the target surface in a narrow cone angle with respect to the target normal [14]. This results in cylindrical geometry for fs-LA plumes at high pressures due to less confinement in the plume expansion direction in comparison to the axial direction. Even though both plumes showed differences in internal structures and changes in aspect ratios with respect to background pressure levels, both plumes decelerate with increasing pressure. Several reports exist on predicting plume propagation at various pressure levels using shock wave, drag and Predtechensky and Mayorov (PM) models and these models describe plume expansion front position with respect to time at different levels of background pressure regardless of pulse duration of laser excitation [17–22].

Figure 2 gives typical time-integrated spectra recorded at various pressure levels. The spectra are recorded at a distance of 1 mm from the target in a time-integrated manner with 100-ns delay and 1-μs gate width. Typically, significant continuum emission is observed for ns-LA at early times (<100 ns) even at vacuum and this continuum emission is significantly lower for fs-LA. The fs-LA spectra are dominated by excited neutrals regardless of the pressure levels, while significant variations in spectral features are noticeable for ns-LA. In both cases, the background was enhanced significantly with increasing ambient pressure. For fs-LA, Coulomb explosion, phase explosion, fragmentation and thermal vaporization are the main mechanisms responsible for the ablation [6]. Thermal vaporization is responsible for the generation of excited neutral species within the plume, as these species appear near to the vaporization temperature of the target material, and hence produce a plume consisting largely of excited neutral atomic species [4, 23, 24]. In the ns-LA spectra, along with excited neutral lines, ionic and ambient gas lines are also present. In ns LPP, the laser–plasma heating is prevalent after the initial generation of the laser ablation plume, which will enhance further ionization of the bulk plasma, intense continuum generation, and background gas ionization and plasma generation.

Figure 3 gives the intensity variation of a characteristic Cu I line at 510.5 nm ($4p^2P_{3/2}$–$4s^2D_{5/2}$) at various ambient air pressure levels. The measurement given in Fig. 3 corresponds to recorded line intensity at a distance 1 mm from the target with an integration time of 1 μs. Considering typical velocities of plasma species $\sim 5 \times 10^5$ to 5×10^6 cm/s [25], it has to be mentioned that the emission intensities of all lines peak at a time <1 μs at 1 mm after the onset of plasma formation. The line intensities are lower at vacuum and at lower background pressure levels due to large mean free paths and free expansion of the plume, resulting in decreased collisions between species and lower temperature. Both ns- and fs-LA plume intensities started to increase rapidly from moderate pressure levels (>100 mTorr), where the ambient gas collisional effects between the plume species and ambient gas species start to play a significant role in excitation/de-excitation of species and confinement of the plume [26]. This causes spectral line intensities to grow with increasing pressure and attain a maximum value near to atmospheric pressure levels, and then decrease again at higher-pressure levels. The decrease

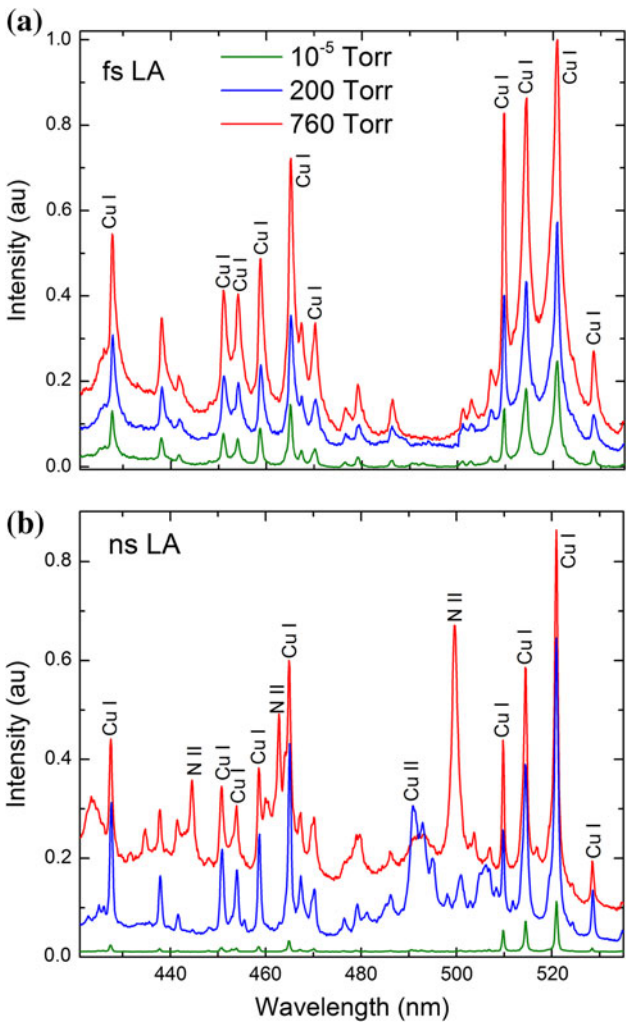

Fig. 2 Representative emission spectra from **a** fs-LA and **b** ns-LA are given at various pressure levels. The spectra are recorded at a distance 1 mm from the target in a time-integrated manner after 100-ns delay and with 1-μs gate width. The *assigned lines* are marked

in intensity at higher pressures could be attributed to decrease in temperature due to an increased recombination. However, the optimum pressure conditions where the maximum signal is observed are found to be slightly different for ns- and fs-LA plumes (~600 Torr for ns-LA and ~300 Torr for fs-LA). Both plasmas are spatially confined by the background gas medium under these pressure conditions based on ICCD imaging results. The plasma excitation caused by confinement will enhance with increasing pressure, however at higher-pressure levels, energy dissipation of plume can also be caused by non-radiative means. It has to be specified that the optimal signal conditions will be highly dependent on laser parameters as well as emission collection system and will vary for different conditions.

Though the signal intensity achieved its peak value at background pressure levels of ~300 to 600 Torr for ns- and fs-LA plumes, it is not necessarily true that these are the best conditions for analytical applications like LIBS, considering differences in background continuum emission for short (ns) and ultrashort (fs) LA. The background continuum is significantly higher for ns-LA compared to fs-LA even at vacuum conditions due to the laser–plasma coupling and increased plume ionization that occurs during ns-LA and is absent during fs-LA. Because there is only laser–target coupling in fs-LA, energetic ionized species and electrons produced through the Coulomb explosion mechanism escape from the target at very early times and are not present within the bulk plasma plume that contains mostly excited neutral species produced primarily through thermal vaporization. The calculated signal to background ratios (S/B) at different pressure levels are given in Fig. 4. According to Fig. 4, the S/B increases with the reduction of pressure from atmospheric level and is maximized in pressure range ~20 to 50 Torr for both ns- and fs-LA plumes. The observation of optimum analytical merits at pressure levels ~20 to 50 Torr could be due to an interplay between improved signal intensity because of collisional and confinement effects at these pressures coupled with limited background continuum emission, while background emission increases substantially at higher-pressure levels. For optical collection parameters investigated in this article, the fs-LA plumes are found to provide relatively higher S/B from vacuum conditions to pressure ~200 Torr because of reduced continuum emission compared to ns-LA. However, at higher-pressure levels (~>200 Torr), the S/B from the ns-LA supersedes the fs-LA, most likely due to increasing absolute signal intensity with a disproportionate increase in background emission as pressure levels continue to increase. Our recent results showed that we can obtain significantly higher S/B even for ns-LA at atmospheric conditions with the use of longer collection delays (~1 μs) after the onset of plasma formation, allowing for decay of background continuum emission [27].

The absolute signal intensities and S/B showed optimum conditions at different pressure levels, however both occur at relatively moderate to higher-pressure levels. At these pressure levels, both the ns- and fs-LA plumes are confined considerably because of ambient gas pressure, and hence the changes in signal intensity and background level could be related to changes in plasma temperature with respect to pressure. Therefore, we estimated the excitation temperature in the plasma using the Boltzmann method, employing

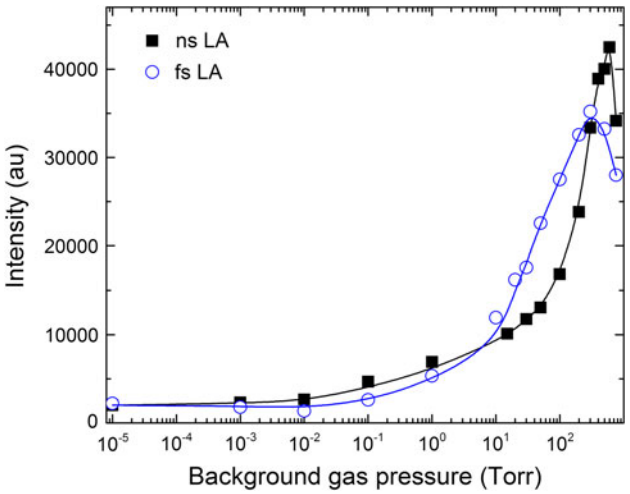

Fig. 3 The variation of absolute intensity of Cu I 510.5 nm line from ns and fs laser ablation plumes at various pressure levels. The measurements were done at a distance 1 mm from the target and with an integration time of 1 μs and a delay of 100 ns. Maximum error corresponds to 10 % of the measured value

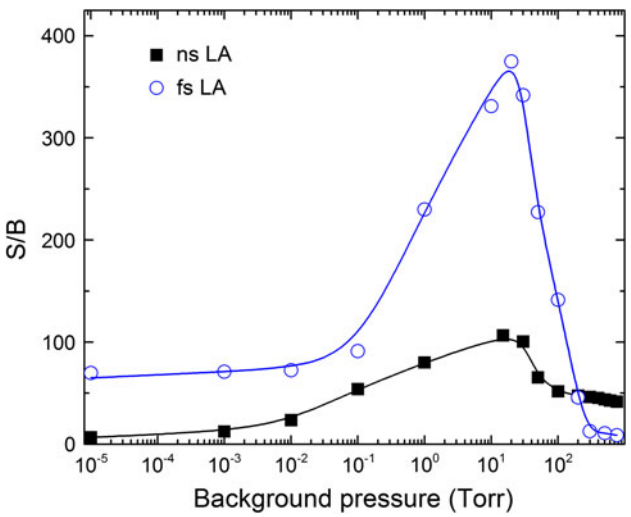

Fig. 4 The S/B as a function of background air pressure for Cu I emission line at 510.5 nm for ns and fs Cu laser ablation plume. The measurements were performed at a distance 1 mm from the target surface with an integration time of 1 μs and a delay of 100 ns

427, 465, 510, 515, and 521 nm Cu I emission lines and results are given in Fig. 5. This measurement was done at 1 mm from the target with an integration time of 1 μs and a delay of 100 ns for both ns and fs plumes. At a distance 1 mm from the target, collisional effects will dominate over radiative processes at low or high ambient pressure

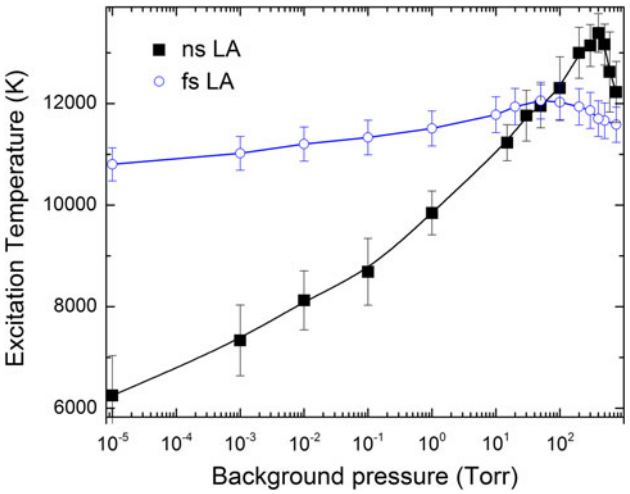

Fig. 5 The role of background air pressure on excitation temperature of Cu plasma

levels which imply that LTE conditions are valid. The temperature variation trend approximately follows the absolute signal intensity curve with respect to pressure given in Fig. 3. At lower pressure levels, the estimated excitation temperature of fs-LA is found to be higher compared to ns-LA. However, the changes in temperature of the fs-LA plume are marginal compared to ns-LA, where the excitation temperature values are increased more than 2× when the pressure increased from vacuum to near atmospheric conditions. At pressures >30 Torr, the time-averaged temperatures of ns-LA are found to be higher than fs-LA. Along with temperature increase, the ambient gas confinement will lead to electron density enhancement [27–29] which in turn enhances the laser–plasma coupling (reheating) through inverse Bremsstrahlung, which has a dependence of N_e^2. The ambient gas plays a more significant role in laser–target and laser–plasma coupling in the case of ns-LA, while in fs-LA, the role of ambient gas is limited to collisional excitation. This is also evidenced in the crater images where the presence of ambient gas made a less significant effect on the crater morphology in fs-LA plumes compared to ns-LA plumes (Fig. 6).

Comparing the crater morphologies given in Fig. 6, the ns-LA craters showed drastic differences in images

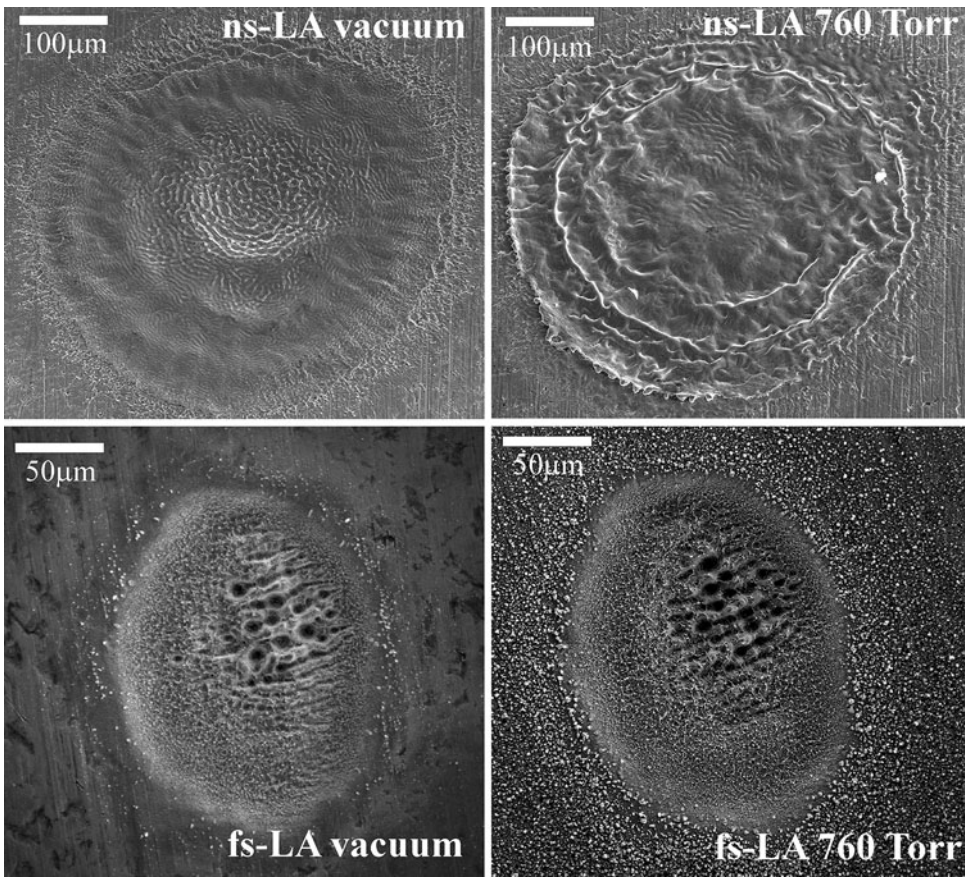

Fig. 6 The SEM images of the ns- and fs-LA crater images after 100 laser shots obtained in vacuum (*left*) and atmospheric air (*right*) conditions

obtained in vacuum and atmosphere conditions. The common features at atmosphere and in vacuum are the re-solidification of molten material. In the presence of background gas, plasma shielding becomes dominant, which not only reduces the mass ablation, but also absorbs the energy from the incoming laser, resulting in higher temperature plasma in front of the target surface (Fig. 5). This hot plasma may enhance the pressure on the molten surface, which may cause splashing, and enhances the material movement from center to periphery of the treated area. Nanosecond LA at vacuum results in smooth crater morphology with maximum ablation at the center due to Gaussian beam profile. In the presence of the ambient gas, ripple formation occurs due to interaction of the melt surface with ambient. In addition, reduced ablation at the center of the crater is observed due to plasma shielding effects at higher pressures. Crater morphology for ns-LA has been studied and it has been shown that vaporization plasma recoil pressure and thermo-capillary convection forces (Marangoni flow) drive the flow of the molten material on the surface, leading to formation of wave-like structures moving away from the craters [30]. Non-linear hydrodynamic instabilities present in plume expansion are also exhibited in crater morphology [30].

The crater morphologies for fs-LA under vacuum and ambient gas cases are similar; however, re-deposited small particles can be seen around the crater in the presence of background gas because of the plasma confinement effect. Ambient pressure and presence of shockwave plays a crucial role in crater morphology as it is the plasma pressure, which dictates the movement of the melt fluid [31–34]. The structures observed in the center of the fs-LA crater, present in both vacuum as well as atmospheric pressure case, have also been observed previously by Bonse et al. [35]. Depending on the laser fluence and number of laser pulses, various morphological structures can be obtained which are determined by various processes including amorphization, annealing and ablation [35].

4 Conclusions

We investigated the background gas pressure effects on expanding ns- and fs-LA plumes. ICCD images highlighted the differences in plume morphologies in the presence of varying ambient pressures which included enhanced emission, plume splitting and sharpening, shockwave formation, confinement, etc. Though the spectral studies showed significant enhancement for all species in the plume and optimum conditions for maximum emission are found to be at $\sim$300 and $\sim$600 Torr, respectively, for fs- and ns-LA, the best S/B was observed at $\sim$20 to 50 Torr levels for both plumes because of disproportional continuum emission at higher-pressure levels. The emission spectra content showed significant differences for ns-LA with increasing pressure in the presence of additional ionic and ambient gas lines, while for fs-LA only incremental increase in spectral intensity and continuum was seen. This can be understood considering large differences in excitation temperature with pressure for ns-LA in comparison with fs-LA. The crater morphologies also showed that the ambient gas pressure levels had less influence on the fs laser-generated craters as compared to ns-LA craters. In summary, the pressure of the ambient gas impacts the ns plume more significantly than the fs-LA plume. In fs-LA, the ambient gas affects only collisional excitation and confinement, while for ns-LA, the background pressure affects the laser–target and laser–plasma couplings as well as the plume excitation and confinement mechanisms.

Acknowledgments This work is partially supported by the US DOE National Nuclear Security Administration under award number DE-NA0001174.

References

1. N.L. LaHaye, S.S. Harilal, P.K. Diwakar, A. Hassanein, J. Anal. At. Spectrom. **28**, 1781 (2013)
2. P.K. Diwakar, S.S. Harilal, N.L. LaHaye, A. Hassanein, P. Kulkarni, J. Anal. At. Spectrom. **28**, 1420 (2013)
3. R.E. Russo, X.L. Mao, J.J. Gonzalez, V. Zorba, J. Yoo, Anal. Chem. **85**, 6162 (2013)
4. L. Jiang, H. Tsai, *Femtosecond laser ablation: challenges and opportunities*. in Proceeding of NSF Workshop on Research Needs in Thermal, Aspects of Material Removal, Stillwater, OK (2003)
5. E.G. Gamaly, A.V. Rode, B. Luther-Davies, V.T. Tikhonchuk, Phys. Plasmas **9**, 949 (2002)
6. E.G. Gamaly, *Femtosecond Laser-Matter Interaction: Theory, Experiments and Applications* (Pan Stanford, Singapore, 2012)
7. B. Verhoff, S.S. Harilal, J.R. Freeman, P.K. Diwakar, A. Hassanein, J. Appl. Phys. **112**, 093303 (2012)
8. S.S. Harilal, C.V. Bindhu, M.S. Tillack, F. Najmabadi, A.C. Gaeris, J. Appl. Phys. **93**, 2380 (2003)
9. S.S. Harilal, G.V. Miloshevsky, P.K. Diwakar, N.L. LaHaye, A. Hassanein, Phys. Plasmas **19**, 083504 (2012)
10. A. De Giacomo, M. Dell'Aglio, R. Gaudiuso, S. Amoruso, O. De Pascale, Spectrochim. Acta, Part B **78**, 1 (2012)
11. W. Sdorra, K. Niemax, Mikrochim. Acta **107**, 319 (1992)
12. S.S. Harilal, N. Farid, A. Hassanein, V.M. Kozhevin, J. Appl. Phys. **114**, 203302 (2013)
13. S. Amoruso, G. Ausanio, M. Vitiello, X. Wang, Appl. Phys. A **81**, 981 (2005)
14. B. Verhoff, S.S. Harilal, A. Hassanein, J. Appl. Phys. **111**, 123304 (2012)
15. A. Bogaerts, Z. Chen, Spectrochim. Acta, Part B **60**, 1280 (2005)
16. C. Geertsen, A. Briand, F. Chartier, J.-L. Lacour, P. Mauchien, S. Sjostrom, J.-M. Mermet, J. Anal. At. Spectrom. **9**, 17 (1994)
17. S.H. Jeong, R. Greif, R.E. Russo, Appl. Surf. Sci. **127**, 1029 (1998)
18. S. Amoruso, A. Sambri, X. Wang, Appl. Surf. Sci. **253**, 7696 (2007)

19. A.V. Bulgakov, N.M. Bulgakova, J. Phys. D-Appl. Phys. **31**, 693 (1998)
20. T.E. Itina, J. Hermann, P. Delaporte, M. Sentis, Phys. Rev. E **66**, 066406 (2002)
21. M.R. Predtechensky, A.P. Mayorov, Appl. Supercond. **1**, 2011 (1993)
22. N. Farid, S.S. Harilal, H. Ding, A. Hassanein, Appl. Phys. Lett. **103**, 191112 (2013)
23. R. Stoian, D. Ashkenasi, A. Rosenfeld, E. Campbell, Phys. Rev. B **62**, 13167 (2000)
24. R.F.W. Herrmann, J. Gerlach, E.E.B. Campbell, Appl. Phys. A **66**, 35 (1998)
25. K.F. Al-Shboul, S.S. Harilal, A. Hassanein, J. Appl. Phys. **113**, 163305 (2013)
26. S. George, A. Kumar, R.K. Singh, V.P.N. Nampoori, Appl. Phys. A **98**, 901 (2010)
27. J.R. Freeman, S.S. Harilal, P.M. Diwakar, B. Verhoff, A. Hassanein, Spectrochim. Acta, Part B **87**, 43 (2013)
28. N. Farid, H.B. Wang, C. Li, X.W. Wu, H.Y. Oderji, H.B. Ding, G.N. Luo, J. Nucl. Mater. **438**, 183 (2013)
29. G. Cristoforetti, S. Legnaioli, V. Palleschi, A. Salvetti, E. Tognoni, Spectrochim. Acta, Part B **59**, 1907 (2004)
30. E. György, I.N. Mihailescu, P. Serra, A. Pérez del Pino, J.L. Morenza, Surf. Coat. Technol. **154**, 63 (2002)
31. S. Panchatsharam, B. Tan, K. Venkatakrishnan, J. Appl. Phys. **105**, 093103 (2009)
32. A. Ben-Yakar, A. Harkin, J. Ashmore, R.L. Byer, H.A. Stone, J. Phys. D Appl. Phys. **40**, 1447 (2007)
33. J. Yang, Y. Zhao, N. Zhang, Y. Liang, M. Wang, Phys. Rev. B **76**, 165430 (2007)
34. A. Semerok, B. Sallé, J.-F. Wagner, G. Petite, Laser Part. Beams **20**, 67 (2002)
35. J. Bonse, S. Baudach, J. Kruger, W. Kautek, M. Lenzner, Appl. Phys. A **74**, 19 (2002)